SUPPORTING INFORMATION

Modeling and Upscaling Analysis of Gas Diffusion Electrode-Based Electrochemical Carbon Dioxide Reduction Systems

Ziming Yang[a], Da Li[b,c], Lei Xing[a], Hang Xiang[b], Jin Xuan[c], Shaoan Cheng[d], Eileen Hao Yu[b, c*], Aidong Yang[a*]

[a] *Department of Engineering Science, University of Oxford, Parks Road, Oxford, OX1 3PJ, United Kingdom*

[b] *School of Engineering, Newcastle University, Newcastle Upon Tyne, NE1 7RU, United Kingdom*

[c] *Department of Chemical Engineering, Loughborough University, Loughborough LE11 3TU, United Kingdom*

[d] *State Key Laboratory of Clean Energy Utilization, Zhejiang University, Hangzhou 310027, China*

*Corresponding authors. E-mail address:

aidong.yang@eng.ox.ac.uk;

e.yu@lboro.ac.uk

Number of Pages: 25

Number of Tables: 12

Number of Figures: 6

I. Source terms in the CL

Table S1 Source terms in the CL

Species	Gas-liquid mass transfer	Homogenous reactions	Electrochemical reactions
$CO_2(g)$	$R_{P,CO_2(g)}$	–	–
N_2	–	–	–
H_2	–	–	R_{E,H_2}
CO	–	–	$R_{E,CO}$
$CO_2(aq)$	$R_{P,CO_2(aq)}$	$R_{H,CO_2(aq)}$	$R_{E,CO_2(aq)}$
$HCOO^-$	–	–	$R_{E,HCOO}$
${CO_3}^{2-}$	–	R_{H,CO_3}	–
${HCO_3}^-$	–	R_{H,HCO_3}	–

II. Key parameter values

Table S2 Geometrical parameters in our model

Geometric parameter	Value
GASC thickness, L_{GASC}	5×10^{-3} m
GDL thickness, L_{GDL}	2.1×10^{-4} m
CL thickness, L_{CL}	2×10^{-5} m
ELEC thickness, L_{ELEC}	1.1×10^{-2} m
Electrode height, H_E	1.5×10^{-2} m
Electrode width, W_E	1.3×10^{-2} m
GASC extension length, H_{EXT}	1.5×10^{-3} m
Cathode geometrical surface area, A_C	2×10^{-4} m^2

Table S3 key physicochemical parameter values of the model

	Value	**Ref.**
Gaseous species		
Binary diffusivity of the component $CO_2(g)$ and H_2, $D_{CO_2H_2}$	6.46×10^{-5} m^2 s^{-1}	[1]
Binary diffusivity of the component $CO_2(g)$ and N_2, $D_{CO_2N_2}$	1.65×10^{-5} m^2 s^{-1}	[1]

Binary diffusivity of the component $CO_2(g)$ and CO,D_{CO_2CO}	$1.52 \times 10^{-5}\ m^2\ s^{-1}$	1
Binary diffusivity of the component H_2 and N_2, $D_{H_2N_2}$	$7.79 \times 10^{-5}\ m^2\ s^{-1}$	1
Binary diffusivity of the component H_2 and CO,D_{H_2CO}	$7.43 \times 10^{-5}\ m^2\ s^{-1}$	1
Binary diffusivity of the component CO and N_2,D_{CON_2}	$2.02 \times 10^{-5}\ m^2\ s^{-1}$	1
Aqueous species		
Diffusivity for ${CO_3}^{2-}$, D_{CO_3}	$9.23 \times 10^{-10}\ m^2\ s^{-1}$	1
Diffusivity for $CO_2(aq)$, $D_{CO_2(aq)}$	$1.70 \times 10^{-9}\ m^2\ s^{-1}$*	Calculated
Diffusivity for ${HCO_3}^-$, D_{HCO_3}	$1.185 \times 10^{-9}\ m^2\ s^{-1}$	1
Diffusivity for $HCOO^-$, D_{HCOO}	$5 \times 10^{-10}\ m^2\ s^{-1}$	2
Diffusivity for OH^-, D_{OH}	$5.293 \times 10^{-9}\ m^2\ s^{-1}$	1
Gas-liquid mass transfer		
Henry's constant for CO_2, H_{CO_2}	See below**	Calculated
Mass transfer coefficient for CO_2, K_{GL}	$1 \times 10^{-4}\ m\ s^{-1}$***	
Homogeneous reactions		
Equilibrium constant for the reaction (R4), K_{Ha}	$1 \times 10^{8}\ M^{-1}$	1
Equilibrium constant for the reaction (R5), K_{Hb}	$4.66 \times 10^{3}\ M^{-1}$	3
Forward rate constant for the reaction (R4), k_{Ha}	$1 \times 10^{3}\ M^{-1}s^{-1}$	4
Forward rate constant for the reaction (R5), k_{Hb}	$1 \times 10^{8}\ M^{-1}s^{-1}$	3
Electrode kinetics		
Symmetry factor for the reaction (R1), β_{Ea}	0.4**	
Symmetry factor for the reaction (R2), β_{Eb}	0.4**	1
Symmetry factor for the reaction (R3), β_{Ec}	0.23**	5
Exchange current density of the reaction (R1),$i_{eq,Ea}^{ref}$	$0.90\ A\ m^{-2}$***	6
Exchange current density for the reaction (R2), $i_{o,Eb}^{ref}$	$0.70\ A\ m^{-2}$***	7
Exchange current density for the reaction (R3), $i_{eq,Ec}^{ref}$	$0.015\ A\ m^{-2}$***	5
Reference $CO_2(aq)$ concentration of the reaction (R1), $C_{CO_2(aq),Ea}^{ref}$	1 M	
Reference $CO_2(aq)$ concentration of the reaction (R2), $C_{CO_2(aq),Eb}^{ref}$	1 M	
Standard potential for the reaction (R1), $V_{eq,Ea}^{ref}$ in the reference condition (pH=14)	$-1.02\ V_{SHE}$	8,9

Standard potential for the reaction (R2), $V_{eq,Eb}^{ref}$ in the reference condition (pH=14)	$-0.936\ V_{SHE}$	10,11
Standard potential for the reaction (R3), $V_{eq,Ec}^{ref}$ in the reference condition (pH=14)	$-0.83\ V_{SHE}$	8,9,11

*See section VI for calculation details.

**See section VII for calculation details.

***The values were obtained in this study through parameter fitting by using the experimental data for $0.1M\ KOH$ within the range reported in the cited references.

Table S4 Default values for design and operational parameters

Definition and symbol	Value	Ref.
Universal Parameter		
Density of $CO_2(g)$, $\rho_{CO_2(g)}$	$1.83\ kg\ m^{-3}$	
Density of H_2, ρ_{H_2}	$8.3 \times 10^{-2}\ kg\ m^{-3}$	
Density of N_2, ρ_{N_2}	$1.164\ kg\ m^{-3}$	
Density of CO, ρ_{CO}	$1.164\ kg\ m^{-3}$	
Faraday constant, F	$96485\ C\ mol^{-1}$	
Ideal gas constant, R_{ideal}	$8.314\ J\ mol^{-1}\ K^{-1}$	
Molar weight for CO_2, M_{CO_2}	$4.4 \times 10^{-2}\ kg\ mol^{-1}$	
Molar weight for CO_3^{2-}, M_{CO_3}	$6.0 \times 10^{-2}\ kg\ mol^{-1}$	
Molar weight for H_2, M_{H_2}	$2 \times 10^{-3}\ kg\ mol^{-1}$	
Molar weight for $HCOO^-$, M_{HCOO}	$4.5 \times 10^{-2}\ kg\ mol^{-1}$	
Molar weight for OH^- , M_{OH}	$1.7 \times 10^{-2}\ kg\ mol^{-1}$	
Molar weight for CO, M_{CO}	$2.8 \times 10^{-2}\ kg\ mol^{-1}$	
Molar weight of N_2, M_{N_2}	$1.4 \times 10^{-2}\ kg\ mol^{-1}$	
Valence of CO_3^{2-}, z_{CO_3}	-2	
Valence of HCO_3^-, z_{HCO_3}	-1	

Valence of $HCOO^-$, z_{HCOO}	-1	
Operating Setting Parameters		
Electrolyte volumetric flow rate, q_l	For $V_C = -0.17 \sim -0.77\ V_{RHE}$: $0.25\ ml\ min^{-1}$; For $V_C = -0.77 \sim -1.17\ V_{RHE}$, $0.5\ ml\ min^{-1}$	[7]a
Default feed gas velocity, $u^0_{g,in}$	$3.85 \times 10^{-3}\ m\ s^{-1}$	[7]a
Molar fraction of $CO_2(g)$ in feed gas, $x_{CO_2(g),in}$	99.99%	[7]a
Molar fraction of N_2 in feed gas, $x_{N_2,in}$	0.01%	[7]a
Operating temperature, T	$293\ K$	[7]a
Saturation coefficient in the CL, S_{CL}	0.5	Calculated
Saturation coefficient in GDL, S_{GDL}	0	Assumed
Design Parameters		
Catalyst nanoparticle diameter, d_{cat}	$1 \times 10^{-7}\ m$	[7]a
Cathode potential, V_C	$-0.17 \sim 1.17\ V_{RHE}$*	[7]a
Cross section area of ELEC, A_{ELEC}	$1.43 \times 10^{-4}\ m^2$	b
Cross section area of GASC, A_{GASC}	$6.5 \times 10^{-5}\ m$	b
Density of catalyst, ρ_{cat}	$6.2 \times 10^{3}\ kg\ m^{-3}$	b
Intrinsic electronic conductivity in the CL, $\sigma^0_{s,CL}$	$7.27 \times 10^{4}\ S\ m^{-1}$	[12]
Intrinsic electronic conductivity in the GDL, $\sigma^0_{s,GDL}$	$6.8 \times 10^{3}\ S\ m^{-1}$	b
Intrinsic porosity in the GDL, ϵ^0_{GDL}	0.8	[1]
Mass loading of catalyst, m_{cat}	$5\ mg\ cm^{-2}$	a
Mean CL porous radius, $r_{p,CL}$	$3.5 \times 10^{-8}\ m$	[13]
Mean GDL porous radius, $r_{p,DML}$	$7.5 \times 10^{-6}\ m$	[14]
Standard/intrinsic permeability for the GDL, κ^0_{GDL}	$1.34 \times 10^{-12}\ m^2$	[1,15]
Gaseous species		
Dynamic viscosity of mixture gas, μ_g	$1.47 \times 10^{-5}\ Pa\ s$	
Aqueous species		
Electrolyte density, ρ_l	See below**	[16]

Electrolyte potential in the bulk, V_b	$0\ V_{SHE}$	[1]
Intrinsic electrolyte conductivity, σ_l^0	See below**	[7]a

a. Provided by our experiment collaborator;

b. Calculated by experimental data;

* The reversible hydrogen electrode (RHE) potential is obtained by bulk catholyte pH based on the Nernst equation (see section VIII)

** The value varies with electrolyte KOH concentration (see section IX and X);

III. Specific interfacial areas

Assumptions

1. It is assumed that all the pores in the CL are identical and with the same cylinder shape (as shown in the Figure S1);
2. It is assumed that the electrolyte in the CL is evenly distributed throughout the pore and forms an equivalent film (blue portion in the Figure S1) with the thickness of δ_{ele}; typical value of δ_{ele} in a fuel cell is 10nm.[1,17]
3. The gas phase is only trapped within the pores and occupies the rest of pore volume;
4. It is assumed that catalysts are evenly distributed across the CL pores.

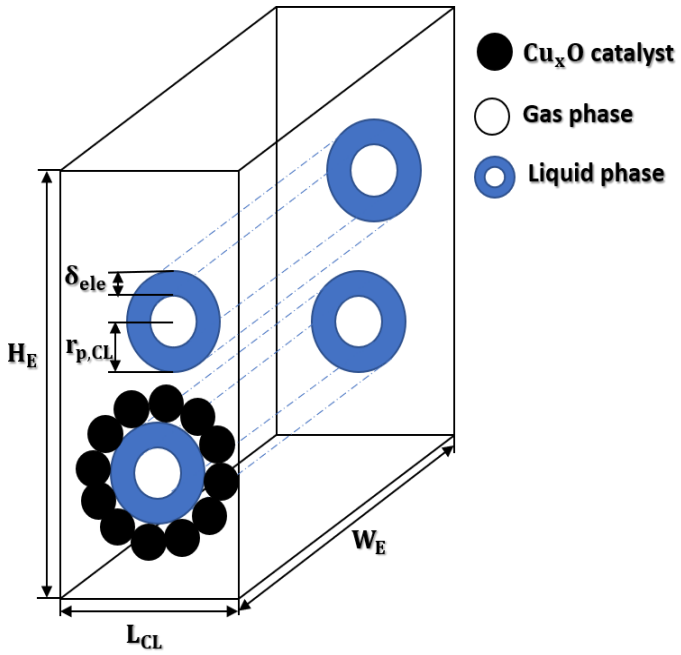

Figure S1 Conceptual schematic of multiphase distribution in the CL.

Calculations

It is assumed that there are n_p pores in the CL. The total pore volume in the CL, V_p is:

$$V_p = \pi r_{p,CL}{}^2 W_E n_p \quad \text{(S1)}$$

The total gas volume in the CL, V_g is:

$$V_g = \pi(r_{p,CL} - \delta_{ele})^2 W_E n_p \quad \text{(S2)}$$

The definition of saturation coefficient in the CL, S_{CL} is:

$$S_{CL} = V_l / V_P \quad \text{(S3)}$$

Based on the third assumption above:

$$V_p = V_l + V_g \tag{S4}$$

The relationship between $r_{p,CL}$, δ_{ele} and S_{CL} is derived by coming Eqs. (S1) to (S4):

$$\delta_{ele} = r_{p,CL}(1 - \sqrt{1 - S_{CL}}) \tag{S5}$$

Eq. (S5) is consistent with the equation reported by the reference[1].

The number of pores in the CL is calculated by Eq. (S1) and the definition for the intrinsic porosity in the CL, ϵ_{CL}^0:

$$n_p = \frac{\epsilon_{CL}^0 V_{CL}}{\pi {r_{p,CL}}^2 W_E} \tag{S6}$$

Thus, the specific interfacial surface area of solid-liquid interface (i.e. total solid-liquid interfacial area per bulk volume of CL), a_{sl} is:

$$a_{sl} = \frac{2\pi r_{p,CL} W_E n_p}{V_{CL}} = 2\frac{\epsilon_{CL}^0}{r_{p,CL}} \tag{S7}$$

Similarly, the specific interfacial surface area of gas-liquid interface (i.e. total gas-liquid interfacial area per bulk volume of the CL), a_{gl} is:

$$a_{gl} = \frac{2\pi(r_{p,CL} - \delta_{ele}) W_E n_p}{V_{CL}} = 2\frac{\epsilon_{CL}^0 (r_{p,CL} - \delta_{ele})}{{r_{p,CL}}^2} \tag{S8}$$

IV. Specific electrical energy consumption (SEEC)

Potential distribution

V_{app} represents the required cell voltage, which is the consequence of the potential drop between the applied cathode potential and theoretical reversible potential adding a series of uncompensated overpotentials (losses):

(i) overall activation overpotential, η_{act} induced by slower electrode kinetics; (ii) overall concentration overpotential, η_{con} due to lower mass transfer and (iii) ohmic overpotential, η_{ohm} describing the resistance of such as electrolyte, membrane to the ions flow. The V_{app} can be obtained according to the voltage balance (see Figure S2) and here we supposed that all calculated V_{app} are below the compliance voltage of the instrument (i.e. potentiostat):

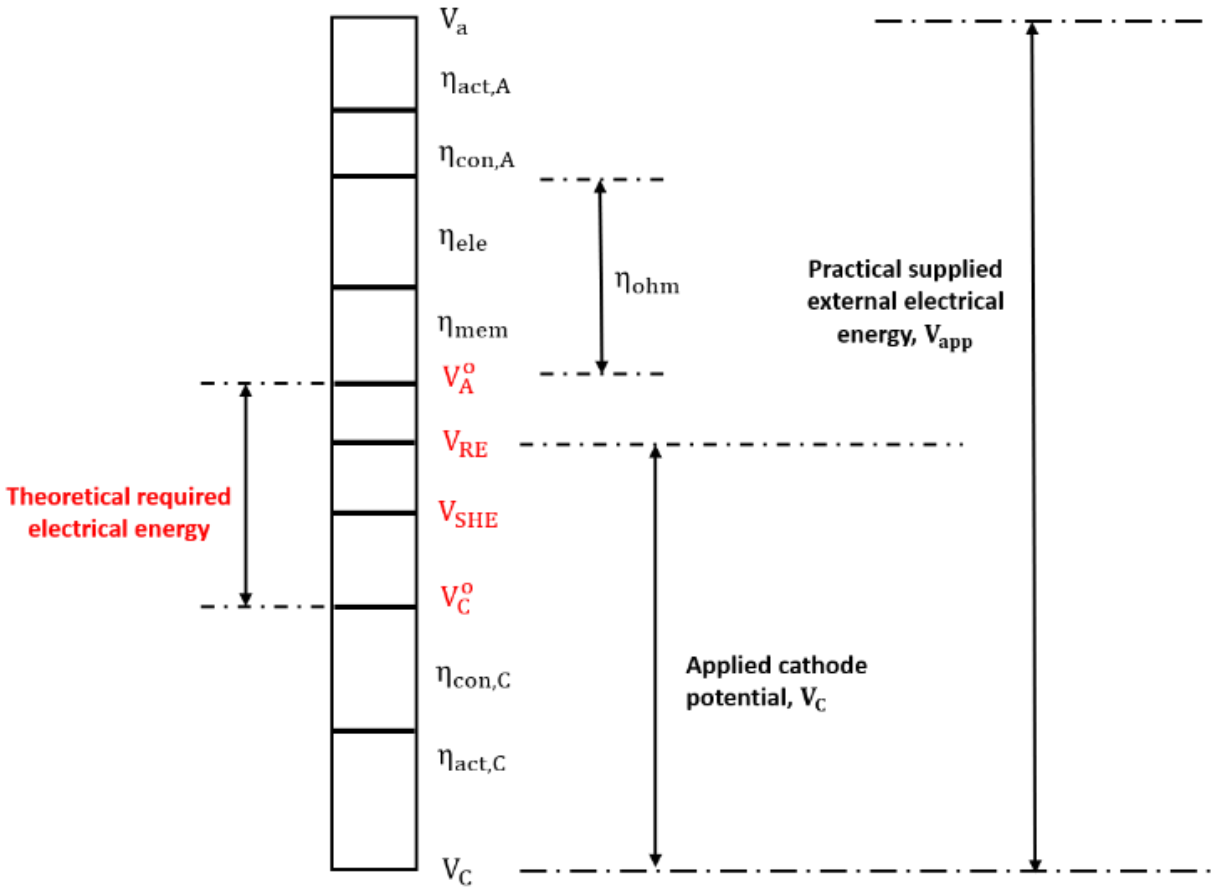

Figure S2 Schematic representation of potential distributions in the three-electrode potentiostat system.

Anodic reaction

Oxygen evolution reaction (OER) takes place at the anode:[7]

$$4OH^- - 4e^- = O_2 + 2H_2O$$

Calculation

$$V_{app} = -(V_C - V_A^o) + \eta_{act,A} + \eta_{con,A} + \eta_{ohm} \quad \text{(S9)}$$

where V_C (negative value) and V_A^o (positive value) are the applied constant cathodic potential and theoretical reversible potential for anodic reaction, respectively; $\eta_{act,A}, \eta_{con,A}$ are the anodic activation overpotential and the anodic concentration overpotential, respectively; η_{ohm} is the ohmic overpotential across the whole cell. Note that V_{app} and all the overpotential terms assume positive values.

Given the relatively slow kinetics of the anodic reaction (i.e. oxygen evolution reaction, OER), its activation overpotential cannot be neglected. It has been proposed that the OER on Platinum (Pt) in the alkaline condition is kinetically controlled by the step of Pt binding hydroxide ion to form the species of $Pt^{\delta} - OH_{ads}$ ($Pt + OH^- = Pt^{\delta} - OH_{ads} + e^-$).[18] Thus, the activation overpotential and concentration overpotential, which have been reported to follow a logarithmic relationship with current density, are approximated by:[9,19,20]

$$\eta_{act,A} = \frac{R_{ideal}T}{\beta_A F} \sinh^{-1}\left(\frac{i_A}{2i_{o,A}}\right) \quad \text{(S10)}$$

$$\eta_{con,A} = -\frac{R_{ideal}T}{n_A F} \ln\left(1 - \frac{i_A}{i_{L,A}}\right) \quad \text{(S11)}$$

where i_A is the current density with respect to the anode geometrical surface area; β_A is the symmetry factor for the anodic reaction, which is set as 0.5 for the method of hyperbolic sine approximation;[19] $i_{o,A}$ and n_A are the exchange current density and the number of transferred electrons for the anodic reaction, respectively. i_A can be linked to the superficial overall current density with respect to the cathode geometrical surface area, i_C by the anode and cathode geometrical surface areas, A_A and A_C:

$$I = i_A A_A = |i_C| A_C \quad \text{(S12)}$$

where I represents the overall current passing though the circuit.

$i_{L,A}$ is the anodic limiting current density corresponding to the maximum reactant consumption rate. Its value is obtained by applying the assumption of no reactant at the reaction site:[9,19]

$$i_{L,A} = \frac{n_A F D_{OH} C_{OH,A,b}}{\delta_d} \quad \text{(S13)}$$

where D_{OH} is the diffusivity for the anodic reactant, OH^-; $C_{OH,A,b}$ is the bulk (anolyte) concentration of the anodic reactant, OH^-; δ_d is the diffusion layer thickness.

For the ohmic overpotential, the resistance caused by the bubble effect on the anode and the circuit are negligible.[21–23] The ohmic overpotential from ions transportation across the electrolyte and membrane is calculated by:[20]

$$\eta_{ohm} = I\left(\frac{1}{\sigma_{ele} L_{AC}} + A_{mem} R_{mem}\right) \quad \text{(S14)}$$

where L_{AC} is the distance between the two electrodes; σ_{ele} is the electrolyte conductivity; A_{mem} and R_{mem} are the geometrical surface area and the specific resistance of the cation exchange membrane (CEM), respectively.

The parameter values for SEEC calculations can be found in the following table and section II.

Parameter values for SEEC calculation

Table S5 Parameter values for SEEC calculation

Definition and symbol	Value	Ref.
SEEC		
Faraday efficiency for $HCOO^-$, FE_{HCOO}	Simulation results	
Theoretical reversible potential for anodic reaction, V_A^o	$+0.40\ V_{SHE}$	[23]

Activation overpotential		
Anode geometrical surface area, A_A	$4\ cm^2$	7
Bulk concentration of the anodic reactant, $C_{OH,A,b}$	$5.0\ M$***	7
Diffusion layer thickness, δ_d	$0.05\ cm$**	24
Distance between anode and cathode, L_{AC}	$2.6\ cm$*	7
Electrolyte conductivity, σ_{ele}	$35\ S\ m^{-1}$***	7
Exchange current density for the anodic reaction (OER), $i_{o,A}$	$1 \times 10^{-7}\ A\ m^{-2}$**	25
Geometrical surface area of CEM, A_{mem}	$3.6\ cm \times 2.4\ cm$	7
Number of transferred electrons of anodic reaction (OER), n_A	4	
Specific resistance of CEM, R_{mem}	$2\ \Omega\ cm^{-2}$**	26
Symmetry factor for anodic reaction (OER), β_A	0.5	19

* The value is derived from experimental data. $L_{AC} = L_A + L_C + L_w$. L_A, L_C, L_w denote the thickness of anodic chamber, cathodic chamber and the plate with window. $L_A = 1.4\ cm;\ L_C = 0.9\ cm; L_w = 0.3\ cm.$

**The value was measured and reported in others' work

- For δ_d: the value used here is the estimated diffusion layer thickness for unstirred solutions, which was reported by the reference;[24]
- For $i_{o,A}$: the value used here was measured from the experiment,[25] where OER takes place on Platinum (Pt) electrode in alkaline condition. In our experiment,[7] the anode was Platinum plated Titanium mesh and $5.0M\ KOH$ was employed as anolyte (i.e. electrolyte in the anode chamber). Given these two experiments[7,25] are similar, the reported value $1 \times 10^{-7}\ A\ m^{-2}$ was directly applied for the calculation;
- For R_{mem}: The value used here was for one of the types of CEM (FKD), measured in 0.5M NaCl solution at $298K$.

*** The values obtained from our experiment together with assumptions:

- For $C_{OH,A,b}$: It is assumed that bulk concentration of anodic reactant, OH^- is constant;
- For σ_{ele}: the values for $2.0M\ KOH$ is employed here by assuming identical electrolyte conductivity for $2.0M\ KOH$ and $5.0M\ KOH$.

Distribution of applied potential

Figure S3 reveals the distribution of the applied potential, V_{app} in detail. One can see that the sum of the ohmic overpotential and the anodic activation overpotential forms a significant part of the potential loss, with the dominance of the latter shifting to that of the former as the applied cathode potential becomes more negative. These losses could be reduced by measures such as the use of superior anode material with faster kinetics, application of the electrolyte with higher conductivity and reduction of the distance between electrodes by using membrane-less cells.

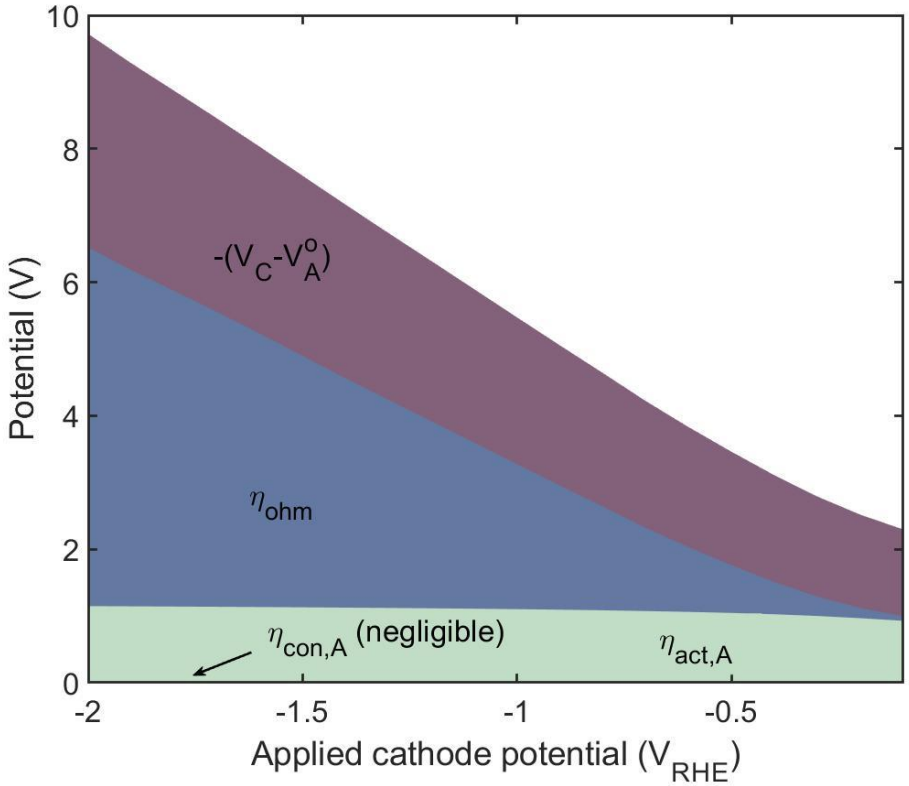

Figure S3 Applied potential distribution.

V. Additional model validation based on $KHCO_3$ electrolyte

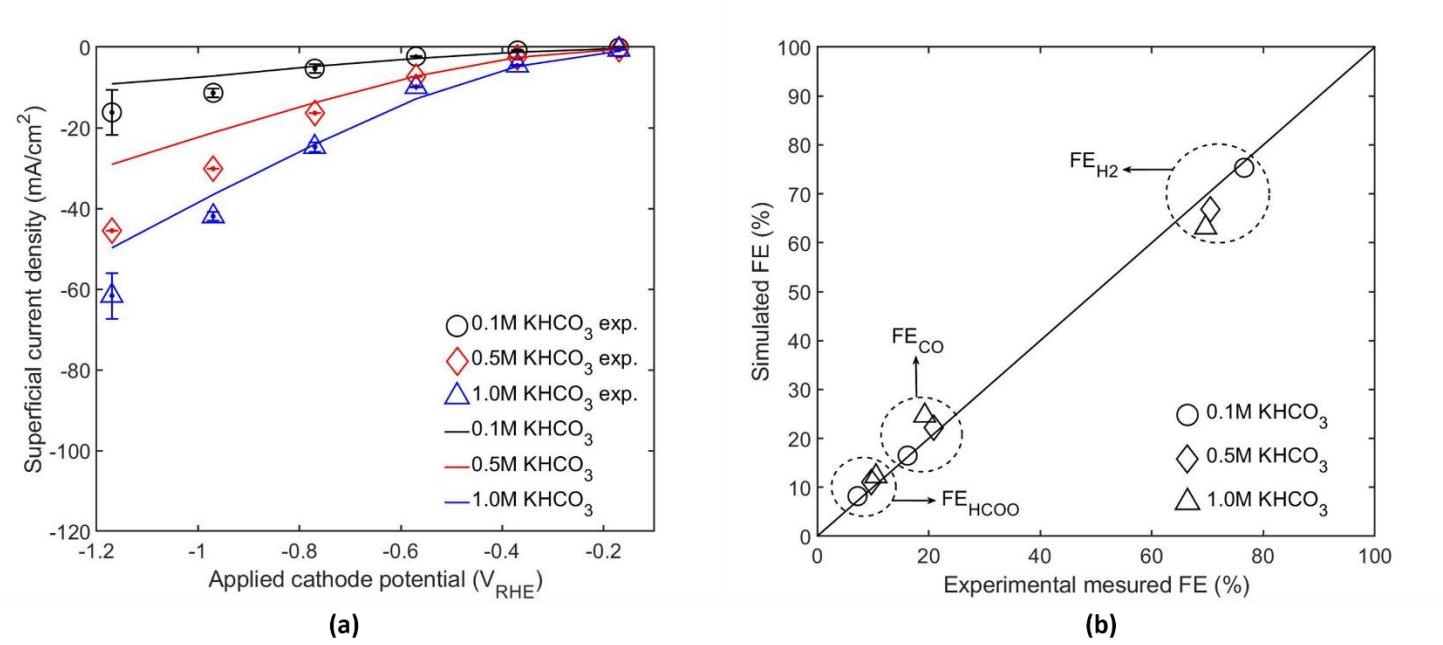

Figure S4 (a) Overall superficial current density with respect to the cathode geometrical surface area; (b) Averaged selectivity from data for different cathode potential levels, with various $KHCO_3$ concentrations, compared with the experimental data.

The experimental data and the detailed experiment setup can be found in the reference.[7] From the Figure S4(b), it is clear that our model is capable of capturing the selectivity (i.e. FE_{HCOO}, FE_{CO} and FE_{H_2}) with very good fidelity for all tested scenarios (i.e. all tested $KHCO_3$ concentrations and values of applied cathodic potential). In terms of the overall superficial current density (Figure S4(a)), our model could predict its value well for all systems (i.e. with all tested $KHCO_3$ concentrations) when the cathode was imposed with relatively positive values. For the system with more negative cathodic potential, the apparent departure of our simulation from experimental results, similar to that observed in the model validation presented in the main text for the system using KOH as the electrolyte, could be attributed to (i) larger random errors of experimental measurements[7] and (ii) more pronounced impact of dynamic changes with increasing current.[7]

VI. $CO_2(aq)$ diffusivity, $D_{CO_2(aq)}$ in various KOH concentration

The diffusivity of dissolved CO_2 in pure water, $D_{CO_2(aq),w}$ is given by:[27]

$$D_{CO_2(aq),w} = 2.35 \times 10^{-6} \exp\left(\frac{-2119}{T}\right) m^2 s^{-1} \quad \text{(S15)}$$

where $T(K)$ is the operating temperature and equals to $293K$ in our case.

The $CO_2(aq)$ diffusivity in various KOH concentrations can be calculated by:[28]

$$\frac{D_{CO_2(aq)}}{D_{CO_2(aq),w}} = 1 - 1.29 \times 10^{-4} C_{OH} \quad \text{(S16)}$$

where C_{OH} (M) is the OH^- concentration. Therefore, the $CO_2(aq)$ diffusivity in various KOH concentrations in our case are obtained and listed in the Table S6.

Table S6 $CO_2(aq)$ diffusivity in various KOH concentration

KOH concentration	$CO_2(l)$ diffusivity in water, $D_{CO_2(aq),w}$ $(m^2 s^{-1})$	$\frac{D_{CO_2(aq)}}{D_{CO_2(aq),w}}$	$CO_2(aq)$ diffusivity in KOH, $D_{CO_2(aq)}$ $(m^2 s^{-1})$
0.1M	1.70×10^{-9}	1.00	1.70×10^{-9}
0.5M		1.00	
1.0M		1.00	
2.0M		1.00	

VII. Calculation of Henry's constant taking into account salting-out effect

The effect of dissolved ionic species on the Henry's constant, known as the salting-out effect.[29–31] For CO_2, H_{CO_2} should be considered when different composition and concentration of electrolyte is employed and compared.[29,30,32]

Combining the Sechenov[30,31] (or written as the German transliteration of 'Setschenow'[29]) relationship that mathematically describes the effect of salinity and the Henry's law, which is applicable for our system,[29,32,33] the Henry's constant is given by:

$$\log \mathrm{H}_{\mathrm{CO}_2} = \log \mathrm{H}_{\mathrm{CO}_2,\mathrm{w}} + \mathrm{k}_\mathrm{s}\mathrm{C}_\mathrm{ele} \tag{S17}$$

where $\mathrm{H}_{\mathrm{CO}_2,\mathrm{w}}$ and $\mathrm{H}_{\mathrm{CO}_2}$ $(\mathrm{Pa\ M^{-1}})$ are the Henry's constant for CO_2in pure water and electrolyte, respectively; k_s $(\mathrm{M^{-1}})$ is the 'Sechenov constant' and C_ele (M) denotes the electrolyte salinity.

As stated in the main text, the fresh electrolyte was continuously supplied through the electrolyte channel and the CL is sufficiently thin, therefore we assume the value of C_ele remains identical to the feed concentration. $\mathrm{H}_{\mathrm{CO}_2,\mathrm{w}}$ can be calculated from the value of Henry's constant in the pure water at the reference temperature ($\mathrm{T^{ref}}$), $\mathrm{H}^{\mathrm{ref}}_{\mathrm{CO}_2,\mathrm{w}}$ using the following correction which is based on the Van't Hoff equation[29,31]

$$\frac{1}{\mathrm{H}_{\mathrm{CO}_2,\mathrm{w}}} = \frac{1}{\mathrm{H}^{\mathrm{ref}}_{\mathrm{CO}_2,\mathrm{w}}} \exp\left(-\frac{\Delta_\mathrm{sol}\mathrm{H}}{\mathrm{R}_\mathrm{ideal}}\left(\frac{1}{\mathrm{T}} - \frac{1}{\mathrm{T^{ref}}}\right)\right) \tag{S18}$$

where $\Delta_\mathrm{sol}\mathrm{H}$ $(\mathrm{J\ mol^{-1}})$ is the enthalpy of dissolution and $\mathrm{R}_\mathrm{ideal}$ $(\mathrm{J\ mol^{-1}\ K^{-1}})$ is the ideal gas constant. The value of $\Delta_\mathrm{sol}\mathrm{H}$ at $\mathrm{T^{ref}}$ has been used for the calculation (note the narrow difference between T, $293\ \mathrm{K}$ and $\mathrm{T^{ref}}$, $298.15\ \mathrm{K}$).

The effect of salinity is actually determined by the dissolved species and ionic strength.[31] For our case, the value of the k_s is given by:[30]

$$k_s = \sum (h_i + h_G)\, n_i \tag{S19}$$

where h_G (M^{-1}) is the gas-specific constant; h_i (M^{-1}) is the ion-specific parameter of ion i and n_i is the index of ion i in the salt formula. Analogous to the Henry's constant, the 'Sechenov constant' varies with temperature and this assumed linear trend can be captured by the S. Weisenberger & A. Schumpe model[30]:

$$h_G = h_G^{ref} + h_T(T - T^{ref}) \tag{S20}$$

where h_G^{ref} (M^{-1}) is the gas-specific constant measured at the reference temperature, T^{ref}; the second term of Eq. (S20) is the correction term for the effect of temperature and h_T $(M^{-1}K^{-1})$ is named as the temperature coefficient here.

It is worthy to mention that the value of k_s remains constant for each of modelled system with various electrolyte, due to the applied isothermal assumption.[30] The parameters used for Henry's constant calculation are listed in the Table S7 and the results are tabulated in the Table S8.

Table S7 Parameter values for H_{CO_2} calculation

	Value	**Ref.**
Reference temperature, T^{ref}	$298.15\ K$	31
The referenced Henry's constant for CO_2 in the pure water, $H_{CO_2,w}^{ref}$	$29\ atm\ M^{-1}$	31
Term of $\frac{-\Delta_{sol}H}{R_{ideal}}$ in the Eq. (S18)	$2400\ K$	31
Ion-specific parameter of K^+, h_{K^+}	$0.0922\ M^{-1}$	30
Ion-specific parameter of OH^-, h_{OH^-}	$0.0839\ M^{-1}$	30
Ion-specific parameter of HCO_3^-, $h_{HCO_3^-}$	$0.0967\ M^{-1}$	30
The referenced gas-specific constant for CO_2, h_G^{ref}	$-0.0172\ M^{-1}$	30
The temperature coefficient for CO_2, h_T	$-0.338 \times 10^{-3}\ M^{-1}K^{-1}$	30

Table S8 Values for H_{CO_2} at various KOH and $KHCO_3$ concentrations

	KOH				$KHCO_3$		
Concentration (M)	0.1	0.5	1.0	2.0	0.1	0.5	1.0
H_{CO_2} $(atm\ M^{-1})$	26	30	35	49	26	30	36

VIII. Reversible hydrogen electrode (RHE) potential

According to the Nernst equation:

$$V_{RHE} = 0 - 0.059pH \quad (S21)$$

It should be noted here that pH value used for Eq. (S21) refers to the pH of bulk catholyte, which are measured by the experiment[7] and listed below:

Table S9 pH of bulk catholyte at various KOH and $KHCO_3$ concentrations

	KOH				$KHCO_3$		
Concentration (M)	0.1	0.5	1.0	2.0	0.1	0.5	1.0
pH	13.02	13.56	13.96	14.30	8.55	9.04	9.67

The constant pH value of bulk catholyte is maintained by supplying fresh electrolyte during the experiment.[7]

IX. Density of different concentrations of aqueous solutions of KOH and $KHCO_3$ at 293K

The density of KOH $(kg\ m^{-3})$ of various molarity (M) at 293K can be calculated based on the following formula:[16]

$$\rho_l = -0.4824M^2 + 45.649M + 1001 \quad (S22)$$

The values of density of KOH and $KHCO_3$ at various concentrations (M) at 293K are summarised below:

Table S10 Values of density of KOH and $KHCO_3$ at various concentrations (M) at 293K

	KOH				$KHCO_3$		
Concentration (M)	0.1	0.5	1.0	2.0	0.1	0.5	1.0
Density ($kg\ m^{-3}$)	1006	1024	1046	1090	1005	1031	1065

X. Values of specific conductivity of KOH and $KHCO_3$ at various concentrations (M)

Table S11 Values of specific conductivity of KOH and $KHCO_3$ at various concentrations (M)

	KOH				$KHCO_3$		
Concentration (M)	0.1	0.5	1.0	2.0	0.1	0.5	1.0
Conductivity ($S\ m^{-1}$)	2.26	10.74	20.13	35.18	1	5	8

The data of specific conductivity for KOH are from the experimental measurements.[7] The data of specific conductivity for $KHCO_3$ are from the literature.[34]

XI. Testing parameter data

Table S12 Testing parameter data

Parameter	Default value	Testing range	Unit
V_C	-0.5	$[-0.1:-0.1:-2.0]$	V_{RHE}
ξ	1*	$[1:5:20]$	Dimensionless
$u_{g,in}$	1**	$[1:1:10]$	$u^0_{g,in}(m\ s^{-1})$
$x_{CO_2(g),in}$	99.99	[60,70,80,90,99.99]	%
ϵ^0_{CL}	0.6	$[0.4:0.1:0.8]$	Dimensionless
m_{cat}	5	$[1:1:5]$	$mg\ cm^{-2}$

* $\xi = 1$ corresponds to the default cathode geometrical surface area of $2 \times 10^{-4}\ m^2$.

**default value for $u^0_{g,in}$ is $3.85 \times 10^{-3}\ m\ s^{-1}$.

XII. Effect of inlet gas composition and velocity

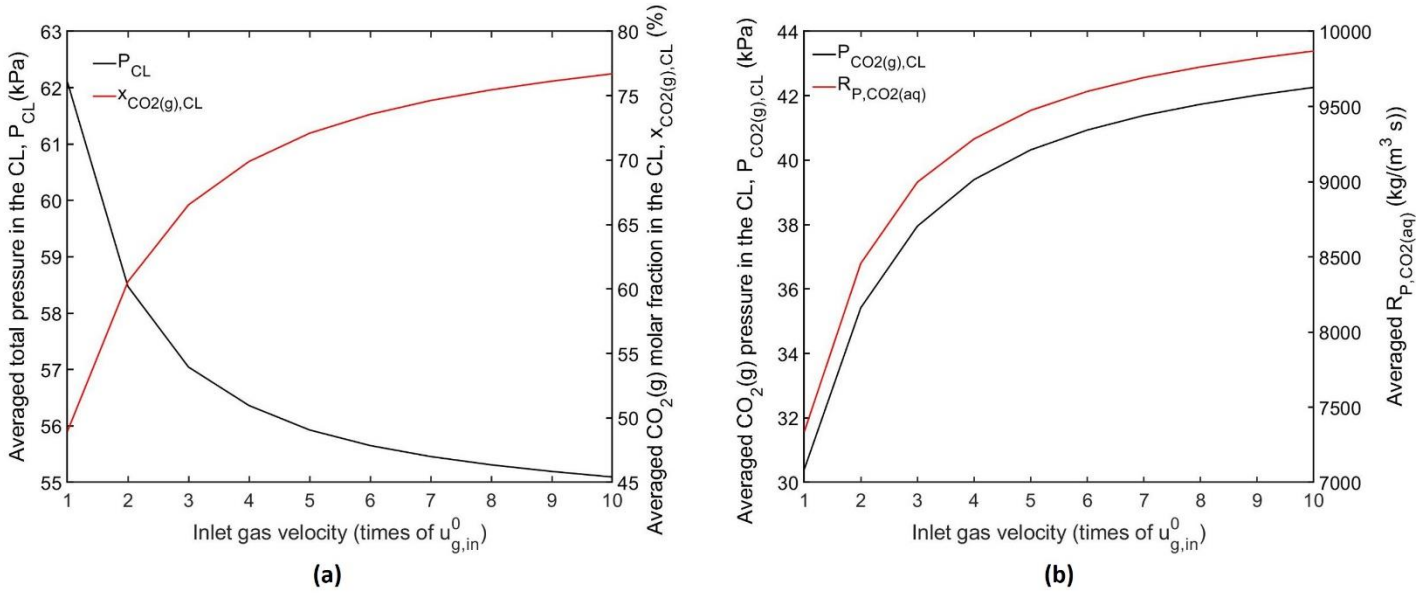

Figure S5 (a) Average total pressure and $CO_2(g)$ molar fraction in the CL and (b) $CO_2(g)$ partial pressure and gas-liquid mass transfer rate in the CL, as the function of inlet gas velocity.

XIII. Effect of catalyst loading and arrangement

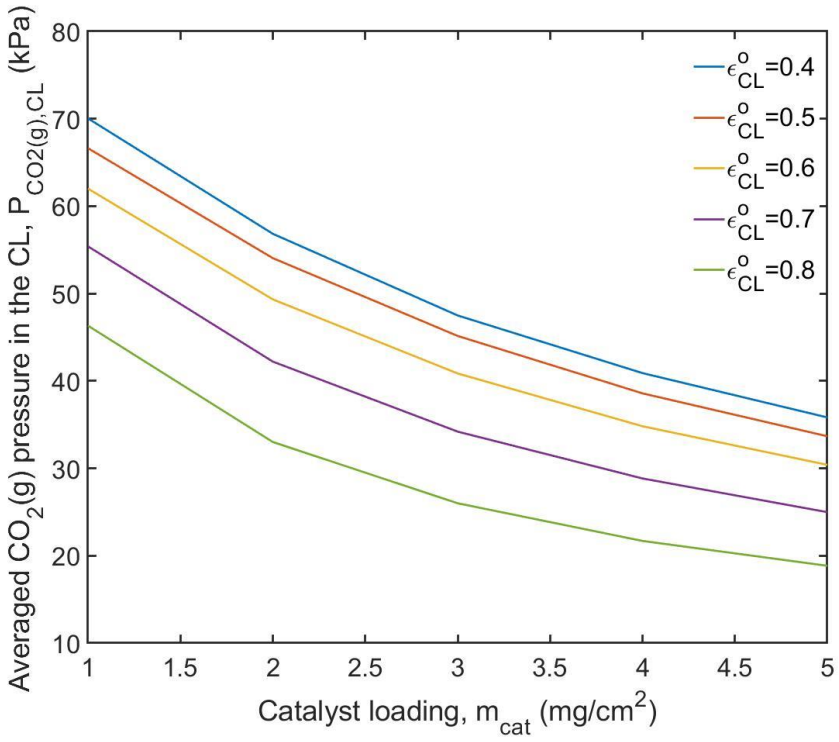

Figure S6 $CO_2(g)$ partial pressure in the CL, as the function of catalyst loading and CL intrinsic porosity.

References

(1) Weng, L. C.; Bell, A. T.; Weber, A. Z. Modeling Gas-Diffusion Electrodes for CO2 Reduction. *Phys. Chem. Chem. Phys.* **2018**, *20*, 16973–16984, DOI 10.1039/c8cp01319e.

(2) Wang, H.; Leung, D. Y. C.; Xuan, J. Modeling of a Microfluidic Electrochemical Cell for CO2 Utilization and Fuel Production. *Appl. Energy* **2013**, *102*, 1057–1062, DOI 10.1016/j.apenergy.2012.06.020.

(3) Suter, S.; Haussener, S. Optimizing Mesostructured Silver Catalysts for Selective Carbon Dioxide Conversion into Fuels. *Energy Environ. Sci.* **2019**, *12*, 1668–1678, DOI 10.1039/c9ee00656g.

(4) Weng, L. C.; Bell, A. T.; Weber, A. Z. Towards Membrane-Electrode Assembly Systems for CO2 Reduction: A Modeling Study. *Energy Environ. Sci.* **2019**, *12*, 1950–1968, DOI 10.1039/c9ee00909d.

(5) Sheng, W.; Myint, M.; Chen, J. G.; Yan, Y. Correlating the Hydrogen Evolution Reaction Activity in Alkaline Electrolytes with the Hydrogen Binding Energy on Monometallic Surfaces. *Energy Environ. Sci.* **2013**, *6*, 1509–1512, DOI 10.1039/c3ee00045a.

(6) Qiao, J.; Fan, M.; Fu, Y.; Bai, Z.; Ma, C.; Liu, Y.; Zhou, X. D. Highly-Active Copper Oxide/Copper Electrocatalysts Induced from Hierarchical Copper Oxide Nanospheres for Carbon Dioxide Reduction Reaction. *Electrochim. Acta* **2015**, *153*, 559–565, DOI 10.1016/j.electacta.2014.09.147.

(7) Xiang, H.; Rasul, S.; Scott, K.; Portoles, J.; Cumpson, P.; Yu, E. H. Enhanced Selectivity of Carbonaceous Products from Electrochemical Reduction of CO2 in Aqueous Media. *J. CO2 Util.* **2019**, *30*, 214–221, DOI 10.1016/j.jcou.2019.02.007.

(8) Li, H.; Oloman, C. Development of a Continuous Reactor for the Electro-Reduction of Carbon Dioxide to Formate - Part 2: Scale-Up. *J. Appl. Electrochem.* **2007**, *37*, 1107–1117, DOI 10.1007/s10800-007-9371-8.

(9) Qiao, J.; Liu, Y.; Zhan, J. *Electrochemical Reduction of Carbon Dioxide: Fundamentals and Technologies*; Taylor & Francis, 2016.

(10) Verma, S.; Lu, X.; Ma, S.; Masel, R. I.; Kenis, P. J. A. The Effect of Electrolyte Composition on the Electroreduction of CO2 to CO on Ag Based Gas Diffusion Electrodes. *Phys. Chem. Chem. Phys.* **2016**, *18*, 7075–7084, DOI 10.1039/c5cp05665a.

(11) Jeanty, P.; Scherer, C.; Magori, E.; Wiesner-Fleischer, K.; Hinrichsen, O.; Fleischer, M. Upscaling and Continuous Operation of Electrochemical CO2 to CO Conversion in Aqueous Solutions on Silver Gas Diffusion Electrodes. *J. CO2 Util.* **2018**, *24*, 454–462, DOI 10.1016/j.jcou.2018.01.011.

(12) Wu, K.; Birgersson, E.; Kim, B.; Kenis, P. J. A.; Karimi, I. A. Modeling and Experimental Validation of Electrochemical Reduction of CO2 to CO in a Microfluidic Cell. *J. Electrochem. Soc.* **2015**, *162* (1), F23–F32, DOI 10.1149/2.1021414jes.

(13) Sabharwal, M.; Pant, L. M.; Putz, A.; Susac, D.; Jankovic, J.; Secanell, M. Analysis of Catalyst Layer Microstructures: From Imaging to Performance. *Fuel Cells* **2016**, *16* (6), 734–753, DOI 10.1002/fuce.201600008.

(14) Ostadi, H.; Rama, P.; Liu, Y.; Chen, R.; Zhang, X. X.; Jiang, K. 3D Reconstruction of a Gas Diffusion Layer and a Microporous Layer. *J. Memb. Sci.* **2010**, *351*, 69–74, DOI 10.1016/j.memsci.2010.01.031.

(15) Zenyuk, I. V.; Medici, E.; Allen, J.; Weber, A. Z. Coupling Continuum and Pore-Network Models for Polymer-Electrolyte Fuel Cells. *Int. J. Hydrogen Energy* **2015**, *40*, 16831–16845, DOI 10.1016/j.ijhydene.2015.08.009.

(16) Gilliam, R. J.; Graydon, J. W.; Kirk, D. W.; Thorpe, S. J. A Review of Specific Conductivities of Potassium Hydroxide Solutions for Various Concentrations and Temperatures. *Int. J. Hydrogen Energy* **2007**, *32*, 359–364, DOI 10.1016/j.ijhydene.2006.10.062.

(17) Cetinbas, F. C.; Ahluwalia, R. K.; Kariuki, N.; De Andrade, V.; Fongalland, D.; Smith, L.; Sharman, J.; Ferreira, P.; Rasouli, S.; Myers, D. J. Hybrid Approach Combining Multiple Characterization Techniques and Simulations for Microstructural Analysis of Proton Exchange Membrane Fuel Cell Electrodes. *J. Power Sources* **2017**, *344*, 62–73, DOI 10.1016/j.jpowsour.2017.01.104.

(18) Favaro, M.; Valero-Vidal, C.; Eichhorn, J.; Toma, F. M.; Ross, P. N.; Yano, J.; Liu, Z.; Crumlin, E. J. Elucidating the Alkaline Oxygen Evolution Reaction Mechanism on Platinum. *J. Mater. Chem. A* **2017**, *5*, 11634–11643, DOI 10.1039/c7ta00409e.

(19) Noren, D. A.; Hoffman, M. A. Clarifying the Butler-Volmer Equation and Related Approximations for Calculating Activation Losses in Solid Oxide Fuel Cell Models. *J. Power Sources* **2005**, *152*, 175–181, DOI 10.1016/j.jpowsour.2005.03.174.

(20) Givirovskiy, G.; Ruuskanen, V.; Ojala, L. S.; Lienemann, M.; Kokkonen, P.; Ahola, J. Electrode Material Studies and Cell Voltage Characteristics of the in Situ Water Electrolysis Performed in a PH-Neutral Electrolyte in Bioelectrochemical Systems. *Heliyon* **2019**, *5*, e01690, DOI 10.1016/j.heliyon.2019.e01690.

(21) Kim, H.; Hwang, H.; Baek, S.; Kim, D. Design, Fabrication and Performance Evaluation of a Printed-Circuit-Board Microfluidic Electrolytic Pump for Lab-on-a-Chip Devices. *Sensors Actuators, A Phys.* **2018**, *277*, 73–84, DOI 10.1016/j.sna.2018.04.042.

(22) Zeng, K.; Zhang, D. Recent Progress in Alkaline Water Electrolysis for Hydrogen Production and Applications. *Prog. Energy Combust. Sci.* **2010**, *36*, 307–326, DOI 10.1016/j.pecs.2009.11.002.

(23) Wang, M.; Wang, Z.; Gong, X.; Guo, Z. The Intensification Technologies to Water Electrolysis for Hydrogen Production - a Review. *Renew. Sustain. Energy Rev.* **2014**, *29*, 573–588, DOI 10.1016/j.rser.2013.08.090.

(24) Bockris, J. O.; Huq, A. K. M. S. The Mechanism of the Electrolytic Evolution of Oxygen on Platinum. *Proc. R. Soc. London. Ser. A. Math. Phys. Sci.* **1956**, *237* (1209), 277–296, DOI 10.1098/rspa.1956.0177.

(25) Damjanovic, A.; Dey, A.; Bockris, J. O. M. Kinetics of Oxygen Evolution and Dissolution on Platinum Electrodes. *Electrochim. Acta* **1966**, *11*, 791–814, DOI 10.1016/0013-4686(66)87056-1.

(26) Długołecki, P.; Anet, B.; Metz, S. J.; Nijmeijer, K.; Wessling, M. Transport Limitations in Ion Exchange Membranes at Low Salt Concentrations. *J. Memb. Sci.* **2010**, *346*, 163–171, DOI 10.1016/j.memsci.2009.09.033.

(27) Versteeg, G. F.; van Swaal, W. P. M. Solubility and Diffusivity of Acid Gases (CO2, N2O) in Aqueous Alkanolamine Solutions. *J. Chem. Eng. Data* **1988**, *33* (1), 29–34, DOI 10.1021/je00051a011.

(28) Darmana, D.; Henket, R. L. B.; Deen, N. G.; Kuipers, J. A. M. Detailed Modelling of Hydrodynamics, Mass Transfer and Chemical Reactions in a Bubble Column Using a Discrete Bubble Model: Chemisorption of CO2 into NaOH Solution, Numerical and Experimental Study. *Chem. Eng. Sci.* **2007**, *62*, 2556–2575, DOI 10.1016/j.ces.2007.01.065.

(29) Valderrama, J. O.; Campusano, R. A.; Forero, L. A. A New Generalized Henry-Setschenow Equation for Predicting the Solubility of Air Gases (Oxygen, Nitrogen and Argon) in Seawater and Saline Solutions. *J. Mol. Liq.* **2016**, *222*, 1218–1227, DOI 10.1016/j.molliq.2016.07.110.

(30) Weisenberger, S.; Schumpe, A. Estimation of Gas Solubilities in Salt Solutions at Temperatures from 273 K to 363 K. *AIChE J.* **1996**, *42* (1), 298–300, DOI 10.1002/aic.690420130.

(31) Sander, R. Compilation of Henry's Law Constants (Version 4.0) for Water as Solvent. *Atmos. Chem. Phys.* **2015**, *15*, 4399–4981, DOI 10.5194/acp-15-4399-2015, 2015..

(32) Carroll, J. J.; Mather, A. E. The System Carbon Dioxide-Water and the Krichevsky-Kasarnovsky Equation. *J. Solution Chem.* **1992**, *21* (7), 607–621, DOI 10.1007/BF00650756.

(33) Moore, J. C.; Battino, R.; Rettich, T. R.; Handa, Y. P.; Wilhelm, E. Partial Molar Volumes of “Gases” at Infinite Dilution in Water at 298.15 K. *J. Chem. Eng. Data* **1982**, *27*, 22–24, DOI 10.1021/je00027a005.

(34) Rosemount Analytical. *Conductance Data for Commonly Used Chemicals*; 2010; Vol. 44.